



# Reduced volatility of aerosols from surface emission to the top of planetary boundary layer

Quan Liu<sup>1,3</sup>, Dantong Liu<sup>2,\*</sup>, Yangzhou Wu<sup>2</sup>, Kai Bi<sup>1</sup>, Wenkang Gao<sup>4</sup>, Ping Tian<sup>1</sup>, Delong Zhao<sup>1</sup>,  
Siyuan Li<sup>2</sup>, Chenjie Yu<sup>5</sup>, Yunfei Wu<sup>6</sup>, Kang Hu<sup>2</sup>, Shuo Ding<sup>2</sup>, Qian Gao<sup>1</sup>, Fei Wang<sup>1</sup>, Hui He<sup>1,7</sup>,  
5 Mengyu Huang<sup>1,7</sup>, Deping Ding<sup>1</sup>

<sup>1</sup> Beijing Weather Modification Office, Beijing 100089, China

<sup>2</sup> Department of Atmospheric Sciences, School of Earth Sciences, Zhejiang University, Hangzhou, Zhejiang, 310027, China

<sup>3</sup> State Key Laboratory of Severe Weather & Key Laboratory of Atmospheric Chemistry of CMA, Chinese Academy of  
10 Meteorological Sciences, Beijing 100081, China

<sup>4</sup> State Key Laboratory of Atmospheric Boundary Layer Physics and Atmospheric Chemistry, Institute of Atmospheric  
Physics, Chinese Academy of Sciences, Beijing 100029, China

<sup>5</sup> Centre for Atmospheric Sciences, School of Earth and Environmental Sciences, University of Manchester, Manchester M13  
9PL, UK.

15 <sup>6</sup> Key Laboratory of Middle Atmosphere and Global Environment Observation (LAGEO), Institute of Atmospheric Physics,  
Chinese Academy of Sciences, Beijing 100029, China

<sup>7</sup> Field experiment base of cloud and precipitation research in North China, China Meteorological Administration, Beijing,  
101200, China

20 *Correspondence to:* Dantong Liu (dantongliu@zju.edu.cn)

**Abstract.** Aerosols from surface emission can be transported upwards through convective mixing in the planetary boundary  
layer (PBL), subsequently interacting with clouds, serving important sources to nucleate droplets or ice particles. However,  
the evolution of aerosol composition during this vertical transport has yet to be explicitly understood. In this study,  
simultaneous measurements of detailed aerosol compositions were conducted at both sites of urban Beijing (50m a.s.l.) and  
25 HaiTuo mountain (1344m a.s.l.) during wintertime, representing the anthropogenically polluted surface environment and the  
top of PBL respectively. The pollutants from surface emissions were observed to reach the mountain site on daily basis  
through daytime PBL convective mixing. From surface to the top of PBL, we found efficient transport or formation for  
lower-volatile species (black carbon, sulfate and low-volatile organic aerosol, OA); however notable reduction of semi-  
volatile substances, such as the fractions of nitrate and semi-volatile OA reduced by 74% and 76% respectively, during the  
30 upward transport. This implied the mass loss of these semi-volatile species was driven by the evaporation process, which  
repartitioned the condensed semi-volatile substances to gas-phase, when aerosols were transported and exposed to a cleaner



environment. Combining with the oxidation processes, these led to enhanced oxidation state of OA at the top of the PBL compared to surface environment, with an increase of oxygen to carbon atomic ratio by 0.2. Such reduction of aerosol volatility during vertical transport may be important in modifying its viscosity, nucleation activity and atmospheric lifetime.

## 35 **1 Introduction**

Substances in the atmosphere present as aerosol and gas phase, are subject to phase transformation during their lifetime (Pankow, 1994, 1987). The processes thermodynamically determine the production of secondary aerosol mass and the constituents of gases, including the condensation process when gas molecular partition to the condensed phase; or in the opposite, the evaporation process occurs when aerosols were diluted in an environment with lower concentration (Donahue et al., 2006). Hereby their physiochemical properties could be modified, such as the condensation results in enlarging aerosol size (Riipinen et al., 2011; Riipinen et al., 2012) or production of new particle (Zhang et al., 2004; Kulmala et al., 2013); the evaporation led to loss of particulate mass (May et al., 2015; Cubison et al., 2011). These have important impacts in altering the radiative interactions of aerosols, by changing the mass of aerosols hereby the direct radiative impacts (Tsigaridis et al., 2014; Wang et al., 2014), or in the number concentration and the ability of cloud condensation nuclei for the indirect radiative impacts (D'Andrea et al., 2013; Kuang et al., 2009). The repartitioned gases from aerosols during dilution could experience chemical evolution and further contribute to the modification of aerosol properties (Zhang et al., 2007; Robinson et al., 2007).

In regions with intense anthropogenic activities, such as megacities, nitrate and sulfate are dominant inorganic aerosol chemical components due to intensive emissions of gaseous precursors (anthropogenic  $\text{NO}_x$  and  $\text{SO}_2$ ) with secondary formation through photochemical and heterogenous/aqueous reactions (Zhang et al., 2015; Huang et al., 2014; Guo et al., 2014; Sun et al., 2016). Although the formation mechanisms of secondary inorganic aerosol are relatively well understood, OA processing in atmospheric transport process remains poorly characterized (Shrivastava et al., 2017). Organic compounds are ubiquitous in ambient aerosol with a large contribution (20-90%) to submicron aerosol mass loadings, including primary OA (POA) and secondary OA (SOA) (Zhang et al., 2007). During atmospheric aging processes, OA physiochemical properties, such as volatility, hygroscopicity, viscosity, and oxidation state, have been significantly transformed. For example, semi-volatile organic materials are repartitioned to gas phase when ambient vapor partial pressure is lower than that in particle phase, and then those vapors can be further photo-oxidized and produce SOA with lower volatility (Robinson et al., 2007). In addition, SOA tend to dominate the OA mass along with atmospheric aging processes, which modulate OA properties to be more oxidized and hygroscopic (Jimenez et al., 2009).

The vertical transport of aerosol and gases in the PBL from surface to the lower free troposphere (FT) importantly determines the influence of anthropogenic emissions to the upper level of the atmosphere, e.g. aerosols at the upper level of the PBL may have more important feedback effects in influencing the boundary layer dynamics (Li et al., 2017). The aerosol could be upward transported from surface to upper level through daytime convective mixing in the PBL (Garratt, 1994).



65 Previous studies have used aircraft (Liu et al., 2020b; Zhao et al., 2019) or balloon platform (Ran et al., 2016; Li et al., 2015) to in-situ measure the vertical profiles of PBL, however lack of sufficient temporal coverage nor full chemical components. The evolution of aerosol properties during this vertical transport in the PBL on daily-basis is yet to be fully understood. In this study, by simultaneous and continuous measurements of detailed aerosol compositions at both surface and surface-influenced mountain sites, we aim to investigate the modification of compositions during the upward transport in the PBL and explore the generic mechanisms in driving the evolution of chemical composition.

## 70 2 Experimental and methods

### 2.1 Experimental sites

Simultaneous measurements of detailed aerosol compositions (organics, nitrate, sulfate, ammonium, chloride, and black carbon) and gaseous pollutants ( $\text{NO}_x$ ,  $\text{SO}_2$ ,  $\text{CO}$ ,  $\text{O}_3$ ) were conducted during January 6<sup>th</sup> to 22<sup>th</sup>, 2019 at both surface and surface-influenced mountain sites, representing the anthropogenically polluted surface urban environment and the top of the PBL respectively. Figure 1a shows the locations of surface and mountain sites, and the spatial distribution of mean aerosol optical depth during the observation period. The surface site locates in the Institute of Atmospheric Physics, Chinese Academy of Science (IAP, 39.97°N, 116.37°E, 50m a.s.l.), where represents the urban environment in Beijing influenced by intense surface anthropogenic emissions. The mountain site (Haituo mountain, 40.52°N, 115.78°E, 1344 m a.s.l.) locates in the northwest Beijing area, which belongs to Taihang mountains and connects to the continental plateau extended to the west. All aerosol measurements were performed downstream of a  $\text{PM}_{2.5}$  impactor (BGI Inc.) at both sites, and dried by a Nafion tube before splitting to the sample inlets of instruments.

### 2.2 Instrumentation and data analysis

Non-refractory aerosol chemical components including nitrate ( $\text{NO}_3$ ), sulfate ( $\text{SO}_4$ ), ammonium ( $\text{NH}_4$ ), chloride (Cl) and organics (Org) were measured by the high-resolution time-of-flight aerosol mass spectrometer (HR-ToF-AMS, Aerodyne Research Inc.) at each site. The instrument operation, calibration, and data analysis are detailed in the supplement information. Positive matrix factorization (PMF) was performed to identify the primary and secondary sources of OA (Ulbrich et al., 2009; Zhang et al., 2011). Four analogous factors were resolved at both sites (Fig. S3 and S4), including two primary organic aerosol (POA), that is, hydrocarbon-like OA (HOA) from traffic emissions and coal combustion OA (CCOA), and two secondary organic aerosol (SOA), that is, semi-volatile oxidized OA (SV-OOA) and low-volatility oxygenated OA (LV-OOA). Except that, another POA, cooking-related OA (COA) was only resolved from surface OA dataset, which has been frequently reported in urban environments (Zhang et al., 2011). Elemental ratios including oxygen-to-carbon (O/C) and hydrogen-to-carbon (H/C) were determined from analysis of high-resolution mass spectra of OA based on the improved-ambient (I-A) method (Canagaratna et al., 2015). While the elemental ratios were also calculated using the



Aiken-ambient (A-A) method (Aiken et al., 2008) for comparison with previous studies. The elemental ratios reported in this  
95 study are obtained from the I-A method unless otherwise stated.

Black carbon (BC) mass was measured by a single particle soot photometer (SP2, DMT Inc.), following the calibration and  
data analysis processes by Liu et al. (2020). Gaseous pollutants (i.e. NO<sub>x</sub>, SO<sub>2</sub>, CO, and O<sub>3</sub>) were measured by gas analyzers  
(model 42i, 43i, 48i, and 49i, Thermo Scientific Inc.). The PBLH was determined by an enhanced single-lens lidar  
100 ceilometer (CL51, Vaisala Co.), using the retrieval method by Tang et al. (2015). Meteorology variables (RH and  
temperature) were measured using WXT-510 (Vaisala Co.).

### 2.3 Air mass history

Three-dimensional air mass histories were calculated by the Numerical Atmospheric dispersion Modeling Environment  
(NAME) (Jones et al., 2007), which is a lagrangian dispersion model following 3D trajectories of plume parcels by Monte  
Carlo methods. The meteorological data source uses the global configuration of UK Met Office's Unified Model. In order to  
105 calculate the historical air mass contribution, the model release tracer particles at a nominal rate of 1 g s<sup>-1</sup>, with a maximum  
travel time of 24 hours in backward mode from target site (i.e. Haituo mountain site in this study), and the integrated time  
was recorded on a 0.25 ° × 0.25 ° horizontal grid from 0 to 1000 m above the ground, aggregating over all particles for a  
given release period. In this study, the potential source contribution of particles to the mountain site (back to 24 hours) from  
air masses classified as four main regions (Fig. 1b): Local (39-41.5°N, 115-117°E, a square region around central Beijing  
110 covering both measurement sites), West (32-41.5°N, 104-115°E), North (41.5-45°N, 104-121°E), and South (32-39 °N, 115-  
121°E). Figure 1b presents a typical example of westerly dominated air mass from NAME outputs. The particle flux is  
integrated in each segregated region, and contributions of each air mass fractions could be obtained.

## 3 Results and discussions

### 3.1 Upward transport of aerosols around midday

115 We aim to classify the source influences on the mountain site from the local surface emission or wider regional area. Air  
mass history analysis showed pronounced diurnal pattern of local air mass influence (as determined by the NAME dispersion  
model), peaking around midday (11:00-14:00). This maximum local influence was consistent with the most developed  
PBLH (Fig. 1c). This suggested the strongest influence of surface emissions to the mountain through midday convective  
mixing (CM) hereby termed as CM period. For certain period (Jan. 9<sup>th</sup> to 12<sup>th</sup>), westerly air mass continuously influenced the  
120 mountain site (grey bar in Fig. 1d-h), which advected regional pollutants from the polluted high plateau, adding on the  
persistent local emission, termed as regional advection (RA) period.

Figure 2 gives the statistical diurnal variations of aerosol species during CM and RA periods respectively, with species of  
BC, OA, nitrate, sulfate shown in Fig. 2a-d, and PMF-derived organic components in Fig. 2e-h. During CM period, the  
chemically-inert species such as BC, showed clear diurnal pattern on the mountain, with elevated concentration by 82% from



125 midday to early afternoon (Fig. 2a). This pattern was highly consistent with the development of PBLH and local air mass  
contribution. On the surface, lower BC concentration showed at the same hours due to the dilution effect of developed PBL,  
but accumulated towards the surface during nighttime inversion. Notably, BC concentration at 11:00-14:00 on the mountain  
almost matched with that on the surface, suggesting the well mix because of the daytime convective mixing. The inert gas  
CO was also efficiently transported without loss from surface to mountain (Fig. S5c). This means the pollutants, if without  
130 reactions, evaporation or other forms of losses, were able to be efficiently transported upwards from surface to the mountain  
site through the daytime convective mixing.

### 3.2 Loss of semi-volatile particulate mass from surface to mountain

Aerosol chemical compositions showed remarkable differences between both sites even when PBL fully developed (Fig. 3),  
i.e. nitrate (23%) and organics (54%) dominated at surface, while sulfate (23%) and organics (45%) dominated at the top of  
135 PBL. Meanwhile, OA varied from POA-dominated (59%) to SOA-dominated (64%). Statistical analysis in Fig. 4 highlights  
the difference between both sites during the periods of CM midday (11:00-14:00), CM night (23:00-02:00) and RA, where  
CM midday represents the period with the most efficient convective mixing. The matched concentrations of BC and CO  
between surface and mountain demonstrated the capability of boundary layer in upward transporting pollutants in terms of  
atmospheric dynamics. For other species such as organics and nitrate particles (Fig. 2b,c), there was still an enhancement on  
140 the mountain peaking around midday, however the loadings was 61% and 74% lower than the surface at the same hours (Fig.  
2b-c, Fig. 4a). This was in contrast with the almost 100% upward transport of BC by convective mixing at the same time.  
The low-volatile species sulfate at both sites showed no apparent (or only broad) diurnal pattern and matched concentration  
in the midday, consistent with its gas precursor SO<sub>2</sub> (Fig. S5b), indicating their regional feature and the aerosol production  
was not sufficiently rapid to display notable diurnal variation.

145 The diurnal patterns of all PMF-resolved organic components on the mountain presented a midday peak feature at different  
amplitude (Fig. 2e-h), suggesting there was no additional source around the site, and the upward transport processes for these  
components was affected by various factors. Previous studies found POA (e.g. HOA and CCOA) has substantial semi-  
volatile materials and presents relatively high volatility (Cao et al., 2018). The comparison between the two sites showed  
significantly decreased semi-volatile species (i.e. HOA, CCOA and SV-OOA), their concentrations on the mountain were  
150 significantly lower than that at surface by 48%, 24% and 76% in the CM midday, respectively (Fig. 4a-b). The LV-OOA is a  
typical SOA which predominantly exists in aged air mass (Zhang et al., 2011). In contrast with semi-volatile species, the low  
volatile LV-OOA on the mountain showed a poorly defined diurnal pattern and its concentrations in the midday were higher  
than that at surface by 52%, which maybe partially caused by further oxidation of relative fresh species in vertical transport  
process.

155 The results above demonstrated that during vertical transport, the loss of particulate masses only occurred for semi-volatile  
substances (nitrate, POA and SV-OOA), but not for low-volatile species (BC, LV-OOA, sulfate) or inert gas (CO).  
Meanwhile, these losses had occurred in a relatively dry condition without notable wet scavenging (Fig. S6b). This



suggested that the evaporation process may have played an important role in repartitioning the condensed phase rich of semi-volatile species to gas phase, which occurred when the activity of semi-volatile species in condensed phase (molar fraction multiplied by activity coefficient) was higher than the partial vapor pressure (relative to equilibrium vapor pressure of pure substance under certain temperature) (Pankow, 1994, 1987). Given the wintertime for the experiment, the mean temperature shifted from -5.5 to 3.8 °C from surface to mountain in the CM midday (Fig. S6a), which was already sufficiently low for even the most volatile species (i.e. ammonium nitrate) to be in condensed phase (Salo et al., 2011) at both sites. Therefore, the temperature decrease within this low range had not driven appreciable condensation process, but the reduction of ambient concentration at mountain (given no additional sources but only contributed by surface emission) was the main reason leading to the evaporation. Additionally, the RH was quite low at both sites (most of time RH<40%, Fig. S6b), below the deliquescence RH for most substances (Cruz and Pandis, 2000), water vapor may thus had not importantly participated in the phase transformation or chemical reactions during vertical transport.

This evaporation process tended to occur along the path of vertical transport, with higher loss rate when larger gradient of concentration between in condensed phase and ambient air (Donahue et al., 2006; Shrivastava et al., 2006; Robinson et al., 2007). Here we only observed the resultant compositions after being transported to the top of PBL, but at which atmospheric layer this process had mostly occurred remained inconclusive. There may be some production process, e.g. photochemical oxidation around midday, which contributed to some increase of SV-OOA concentration around midday (Fig. 2g). The overall reduced SV-OOA suggested its net loss, which was evaporation prevailed production processes, during upwards transport.

During CM night, pollutants (except O<sub>3</sub>) were mostly accumulated at surface (Fig. 4c) due to local emissions and secondary formation processes occurred in a shallow nighttime PBL and interruption of vertical transport to high layers. Note that, the diurnal variation of surface O<sub>3</sub> showed a significant reduction at night due to rapid consumption by strong NO titration, in contrast with a maintainable high O<sub>3</sub> concentration on the mountain without apparent diurnal pattern (Fig. S5d). For RA period, due to additional input of pollutants from a wider regional region besides the local influence, the diurnal variation at mountain was diminished, but showed enhanced concentrations at all hours (Fig. 2), indicated that robust regional advection process also significantly affects aerosol concentration and variation at high layer. Because the surface site was more influenced by local sources, most species had higher concentrations at surface than mountain, apart from sulfur compounds (SO<sub>2</sub> and sulfate, in Fig. 4d). This implies the possible high-level sulfuric sources, e.g. emissions from industrial stack directly into a higher level in the PBL (Wu et al., 2018; Xu et al., 2014).

### 3.3 Modification on the oxidation state of OA

The Van Krevelen-triangle (VK) diagram (Fig. 5a) could indicate the likely oxidation pathway of OA by investigating different degrees of changes on the oxygen or hydrogen over carbon element ratio, depending on the way of adding functional groups (Van Krevelen, 1950). For example, the replacement of a hydrogen atom with an alcohol/peroxide group (-OH, -OOH) results in a slope of 0, while the replacement of a hydrogen atom with a carboxylic acid group (-COOH) results



in a slope of  $-1$  without fragmentation (C-C bond breaking), and  $-0.5$  with fragmentation (Ng et al., 2010). Results mapping on the H:C versus O:C atomic ratio showed discernible regimes between both sites (Fig. 5a). The surface O:C varied at 0.16-0.75, with an average of  $0.42 \pm 0.09$  ( $0.33 \pm 0.08$  with A-A method), generally consistent with those (0.29-0.41, A-A method) previously reported in Beijing (Xu et al., 2015; Zhang et al., 2014; Sun et al., 2016). Mountain OA showed significantly higher O:C (varied at 0.39 to 0.96, with an average of  $0.62 \pm 0.07$ ) and lower H:C (1.23-1.64) than surface, similar with the regime of LV-OOA dominated periods observed in Rocky Mountain National Park ( $\sim 2740$  m a.s.l.) (Schurman et al., 2015). Here the surface (slope =  $-0.64$ ) showed a steeper slope than mountain (slope =  $-0.33$ ). The surface thus tended to be dominated by the oxidation pathway of  $-\text{COOH}$  addition (without fragmentation) with apparent decrease of H/C, while the OA at mountain tended to be oxidized in mix with alcohol/peroxide and  $-\text{COOH}$  addition (with fragmentation) pathway hereby less decrease on H/C.

Difference of  $m/z$  spectra for each PMF factor between surface and mountain was analyzed to further investigate the chemical modification of OA from each source (Fig. 6). The mountain  $\text{CO}_2^+$  fraction in  $m/z$  spectra of all PMF factors enhanced at various extents, indicating the oxidation by adding carboxyl groups (Ng et al., 2011). For HOA and SV-OOA, a range of hydrocarbon fragments decreased at mountain (Fig. 6a, c), which tended to be consistent with the evaporation mechanism proposed in section 3.2 that semi-volatile species may have been repartitioned to the gas phase when transported to the mountain, and these evaporated species may contain significant fraction of more volatile hydrocarbons (Cappa and Jimenez, 2010). Note that the diurnal variation of mountain O:C characterized by slightly fluctuating at a high value region, in contrast with a distinct peak in the early afternoon appearing in the diurnal variation of surface O:C (Fig. 5b). This implied there was no additional primary emissions on the mountain to contribute either particles or VOCs. Meanwhile, mountain  $\text{O}_3$  concentration maintained at a high level without apparent diurnal pattern, in contrast with prominent diurnal variation of surface  $\text{O}_3$  (Fig. S5d). The maintainable high  $\text{O}_3$  concentration on the mountain meant a high oxidation capability. Thus the repartitioned gas species during upwards transport, in addition to the directly transported VOCs, may be further oxidized by the high level of  $\text{O}_3$  throughout the day and night, and re-condensed on particle phase (Robinson et al., 2007). The continuous oxidation on these vapors potentially contributed to production of SOA, which may partly explain the higher levels of O:C at mountain than surface throughout all hours. The mass spectra of mountain HOA and SV-OOA had substantial reductions mainly at ion series  $\text{C}_x\text{H}_{2x-1}^+$  (Fig. 5b), suggesting the  $\text{O}_3$  oxidation may occur on unsaturated bonds (e.g. alkenes) (Paulson and Orlando, 1996) hereby following a less steep slope on the VK space, consistent with above.

For CCOA and LV-OOA, H:C had a substantial decrease but O:C only increased slightly (Fig. 6b, d). The  $m/z$  difference of CCOA shows substantial decrease of  $\text{C}_x\text{H}_y\text{O}^+$  fragments at mountain, which may compensate some of the O:C increase. Some  $\text{C}_x\text{H}_y^+$  fragments showed increase at mountain, which tended to be consistent with the view that the CCOA is largely contributed by non-local sources (Li et al., 2019). This factor may have not experienced significant vertical transport from the surface, thus showing some fresher signatures (the  $\text{C}_x\text{H}_y^+$  fragments) at mountain. which may be compensated by the substantial decrease of  $\text{C}_x\text{H}_y\text{O}^+$  fragments at mountain. LV-OOA had a large enhancement of  $\text{CHO}^+$  and reduction of  $\text{CH}_2\text{O}^+$ , maybe caused by some transformation of alcohols to carbonyl compounds (Grosjean et al., 1993).



## 225 4 Conclusions and implications

The increase of oxidation state could be caused by the evaporation process by losing the less oxidized and more volatile species, and the evaporated gases could be further oxidized to partition to a more oxidized phase. The evaporative loss had occurred in a relatively short time scale, i.e. a few hours' vertical transported induced by daytime convective mixing of boundary layer, as reflected by 76% decrease of semi-volatile organic masses, and 74% of nitrate. These losses had occurred

230 in a relatively dry condition without notable wet scavenging, therefore the evaporative loss tended to dominate. For the other period on the mountain rather than midday, there was additional primary sources in contributing neither particles nor VOCs, thus most of the vapors repartitioned from the condensed phase in the midday may stay and be subjected to oxidation at the mountain. These continuous inputs of gases to the top of boundary layers on daily basis serve a source of precursors to be oxidized and contribute to an important fraction of highly oxidized SOA.

235 All of these processes lead to a consistent manner in enhancing the oxidation state of OA at the top of PBL, which may modify the hygroscopicity and viscosity of OA (Koop et al., 2011). Combining with the more efficiently transported less-volatile species, these processes consistently led to overall decreased volatility of aerosols at top of the PBL, where cloud formation is initialized, influencing the activities of both cloud condensation nuclei and ice nuclei. This also implies that the aerosol characteristics at surface may not represent that at upper levels, where the evolution during transport should be

240 considered in evaluating the contribution of surface emissions to cloud particle nucleation and their atmospheric lifetime.

**Data availability.** All data in this paper are available from the authors upon request (liuquan620@126.com).

**Author contributions.** DD, MH, and HH led and designed the study. QL, DL, YW, KB, WG, PT, DZ, SL, CY, YW, KH, SD, QG, and FW were involved in collecting, processing and analysis of surface and mountain data. QL and DL carried out

245 the data analysis and wrote the paper. QL and all authors contributed to the discussions.

**Competing interests.** The authors declare that they have no conflict of interest.

250 **Acknowledgments. Acknowledgments.** This work was supported by National Key Research and Development Program of China (No. 2016YFA0602001, 2019YFC0214703), the National Natural Science Foundation of China (No. 41975177, 41875167, 41875044, 41775138), and the Beijing Natural Science Foundation (No. 8192021,8194065).

## References

255 Aiken, A. C., DeCarlo, P. F., Kroll, J. H., Worsnop, D. R., Huffman, J. A., Docherty, K. S., Ulbrich, I. M., Mohr, C., Kimmel, J. R., Sueper, D., Sun, Y., Zhang, Q., Trimborn, A., Northway, M., Ziemann, P. J., Canagaratna, M. R., Onasch, T.





- B., Alfarra, M. R., Prevot, A. S. H., Dommen, J., Duplissy, J., Metzger, A., Baltensperger, U., and Jimenez, J. L.: O/C and OM/OC Ratios of Primary, Secondary, and Ambient Organic Aerosols with High-Resolution Time-of-Flight Aerosol Mass Spectrometry, *Environ. Sci. Technol.*, 42, 4478-4485, 10.1021/es703009q, 2008.
- 260 Canagaratna, M. R., Jimenez, J. L., Kroll, J. H., Chen, Q., Kessler, S. H., Massoli, P., Hildebrandt Ruiz, L., Fortner, E., Williams, L. R., Wilson, K. R., Surratt, J. D., Donahue, N. M., Jayne, J. T., and Worsnop, D. R.: Elemental ratio measurements of organic compounds using aerosol mass spectrometry: characterization, improved calibration, and implications, *Atmos. Chem. Phys.*, 15, 253-272, 10.5194/acp-15-253-2015, 2015.
- Cao, L. M., Huang, X. F., Li, Y. Y., Hu, M., and He, L. Y.: Volatility measurement of atmospheric submicron aerosols in an urban atmosphere in southern China, *Atmos. Chem. Phys.*, 18, 1729-1743, 10.5194/acp-18-1729-2018, 2018.
- 265 Cappa, C. D., and Jimenez, J. L.: Quantitative estimates of the volatility of ambient organic aerosol, *Atmos. Chem. Phys.*, 10, 5409-5424, 10.5194/acp-10-5409-2010, 2010.
- Cruz, C., and Pandis, S.: Deliquescence and Hygroscopic Growth of Mixed Inorganic–Organic Atmospheric Aerosol, *Environ. Sci. Technol.*, 34, 4313-4319, 10.1021/es9907109, 2000.
- 270 Cubison, M. J., Ortega, A. M., Hayes, P. L., Farmer, D. K., Day, D., Lechner, M. J., Brune, W. H., Apel, E., Diskin, G. S., Fisher, J. A., Fuelberg, H. E., Hecobian, A., Knapp, D. J., Mikoviny, T., Riemer, D., Sachse, G. W., Sessions, W., Weber, R. J., Weinheimer, A. J., Wisthaler, A., and Jimenez, J. L.: Effects of aging on organic aerosol from open biomass burning smoke in aircraft and laboratory studies, *Atmos. Chem. Phys.*, 11, 12049-12064, 10.5194/acp-11-12049-2011, 2011.
- D'Andrea, S. D., Häkkinen, S. A. K., Westervelt, D. M., Kuang, C., Levin, E. J. T., Kanawade, V. P., Leaitch, W. R., 275 Spracklen, D. V., Riipinen, I., and Pierce, J. R.: Understanding global secondary organic aerosol amount and size-resolved condensational behavior, *Atmos. Chem. Phys.*, 13, 11519-11534, 10.5194/acp-13-11519-2013, 2013.
- Donahue, N., Robinson, A., Stanier, C., and Pandis, S.: Coupled partitioning, dilution, and chemical aging of semivolatile organics, *Environ. Sci. Technol.*, 40, 2635-2643, 2006.
- Garratt, J. R.: Review: the atmospheric boundary layer, *Earth Sci. Rev.*, 37, 89-134, 1994.
- 280 Grosjean, D., Grosjean, E., and Williams, E. L.: Atmospheric chemistry of unsaturated alcohols, *Environ. Sci. Technol.*, 27, 2478-2485, 10.1021/es00048a026, 1993.
- Guo, S., Hu, M., Zamora, M. L., Peng, J., Shang, D., Zheng, J., Du, Z., Wu, Z., Shao, M., Zeng, L., Molina, M. J., and Zhang, R.: Elucidating severe urban haze formation in China, *Proceedings of the National Academy of Sciences of the United States of America*, 111, 17373-17378, 10.1073/pnas.1419604111, 2014.
- 285 Huang, R.-J., Zhang, Y., Bozzetti, C., Ho, K.-F., Cao, J.-J., Han, Y., Daellenbach, K. R., Slowik, J. G., Platt, S. M., Canonaco, F., Zotter, P., Wolf, R., Pieber, S. M., Bruns, E. A., Crippa, M., Ciarelli, G., Piazzalunga, A., Schwikowski, M., Abbazade, G., Schnelle-Kreis, J., Zimmermann, R., An, Z., Szidat, S., Baltensperger, U., Haddad, I. E., and Prevot, A. S. H.: High secondary aerosol contribution to particulate pollution during haze events in China, *Nature*, 514, 218-222, 10.1038/nature13774, 2014.



- 290 Jimenez, J. L., Canagaratna, M. R., Donahue, N. M., Prevot, A. S. H., Zhang, Q., Kroll, J. H., DeCarlo, P. F., Allan, J. D.,  
Coe, H., Ng, N. L., Aiken, A. C., Docherty, K. S., Ulbrich, I. M., Grieshop, A. P., Robinson, A. L., Duplissy, J., Smith, J. D.,  
Wilson, K. R., Lanz, V. A., Hueglin, C., Sun, Y. L., Tian, J., Laaksonen, A., Raatikainen, T., Rautiainen, J., Vaattovaara, P.,  
Ehn, M., Kulmala, M., Tomlinson, J. M., Collins, D. R., Cubison, M. J., E., Dunlea, J., Huffman, J. A., Onasch, T. B.,  
Alfarra, M. R., Williams, P. I., Bower, K., Kondo, Y., Schneider, J., Drewnick, F., Borrmann, S., Weimer, S., Demerjian, K.,  
295 Salcedo, D., Cottrell, L., Griffin, R., Takami, A., Miyoshi, T., Hatakeyama, S., Shimono, A., Sun, J. Y., Zhang, Y. M.,  
Dzepina, K., Kimmel, J. R., Sueper, D., Jayne, J. T., Herndon, S. C., Trimborn, A. M., Williams, L. R., Wood, E. C.,  
Middlebrook, A. M., Kolb, C. E., Baltensperger, U., and Worsnop, D. R.: Evolution of Organic Aerosols in the Atmosphere,  
*Science*, 326, 1525-1529, 10.1126/science.1180353, 2009.
- Jones, A., Thomson, D., Hort, M., and Devenish, B.: The U.K. Met Office's Next-Generation Atmospheric Dispersion Model,  
300 NAME III, Air Pollution Modeling and Its Application XVII, Boston, MA, 2007, 580-589.
- Koop, T., Bookhold, J., Shiraiwa, M., and Pöschl, U.: Glass transition and phase state of organic compounds: dependency on  
molecular properties and implications for secondary organic aerosols in the atmosphere, *Phys. Chem. Chem. Phys.*, 13,  
19238-19255, 10.1039/C1CP22617G, 2011.
- Kuang, C., McMurry, P. H., and McCormick, A. V.: Determination of cloud condensation nuclei production from measured  
305 new particle formation events, *Geophys. Res. Lett.*, 36, 2009.
- Kulmala, M., Kontkanen, J., Junninen, H., Lehtipalo, K., Manninen, H. E., Nieminen, T., Petäjä, T., Sipilä, M.,  
Schobesberger, S., and Rantala, P.: Direct observations of atmospheric aerosol nucleation, *Science*, 339, 943-946, 2013.
- Li, H., Cheng, J., Zhang, Q., Zheng, B., Zhang, Y., Zheng, G., and He, K.: Rapid transition in winter aerosol composition in  
Beijing from 2014 to 2017: response to clean air actions, *Atmos. Chem. Phys.*, 19, 11485-11499, 10.5194/acp-19-11485-  
310 2019, 2019.
- Li, J., Fu, Q., Huo, J., Wang, D., Yang, W., Bian, Q., Duan, Y., Zhang, Y., Pan, J., Lin, Y., Huang, K., Bai, Z., Wang, S.-H.,  
Fu, J. S., and Louie, P. K. K.: Tethered balloon-based black carbon profiles within the lower troposphere of Shanghai in the  
2013 East China smog, *Atmos. Environ.*, 123, 327-338, <https://doi.org/10.1016/j.atmosenv.2015.08.096>, 2015.
- Li, Z., Guo, J., Ding, A., Liao, H., Liu, J., Sun, Y., Wang, T., Xue, H., Zhang, H., and Zhu, B.: Aerosol and boundary-layer  
315 interactions and impact on air quality, *Natl. Sci. Rev.*, 4, 810-833, 10.1093/nsr/nwx117, 2017.
- Liu, D., Hu, K., Zhao, D., Ding, S., Wu, Y., Zhou, C., Yu, C., Tian, P., Liu, Q., Bi, K., Wu, Y., Hu, B., Ji, D., Kong, S.,  
Ouyang, B., He, H., Huang, M., and Ding, D.: Efficient Vertical Transport of Black Carbon in the Planetary Boundary Layer,  
*Geophys. Res. Lett.*, 47, e2020GL088858, 10.1029/2020gl088858, 2020a.
- Liu, Q., Liu, D., Gao, Q., Tian, P., Wang, F., Zhao, D., Bi, K., Wu, Y., Ding, S., Hu, K., Zhang, J., Ding, D., and Zhao, C.:  
320 Vertical characteristics of aerosol hygroscopicity and impacts on optical properties over the North China Plain during winter,  
*Atmos. Chem. Phys.*, 20, 3931-3944, 10.5194/acp-20-3931-2020, 2020b.
- May, A., Lee, T., McMeeking, G., Akagi, S., Sullivan, A., Urbanski, S., Yokelson, R., and Kreidenweis, S.: Observations  
and analysis of organic aerosol evolution in some prescribed fire smoke plumes, *Atmos. Chem. Phys.*, 15, 6323-6335, 2015.



- Ng, N. L., Canagaratna, M. R., Zhang, Q., Jimenez, J. L., Tian, J., Ulbrich, I. M., Kroll, J. H., Docherty, K. S., Chhabra, P. S.,  
325 Bahreini, R., Murphy, S. M., Seinfeld, J. H., Hildebrandt, L., Donahue, N. M., DeCarlo, P. F., Lanz, V. A., Prévôt, A. S. H.,  
Dinar, E., Rudich, Y., and Worsnop, D. R.: Organic aerosol components observed in Northern Hemispheric datasets from  
Aerosol Mass Spectrometry, *Atmos. Chem. Phys.*, 10, 4625-4641, 10.5194/acp-10-4625-2010, 2010.
- Ng, N. L., Canagaratna, M. R., Jimenez, J. L., Chhabra, P. S., Seinfeld, J. H., and Worsnop, D. R.: Changes in organic  
aerosol composition with aging inferred from aerosol mass spectra, *Atmos. Chem. Phys.*, 11, 6465-6474, 10.5194/acp-11-  
330 6465-2011, 2011.
- Pankow, J. F.: Review and comparative analysis of the theories on partitioning between the gas and aerosol particulate  
phases in the atmosphere, *Atmos. Environ.*, 21, 2275-2283, 1987.
- Pankow, J. F.: An absorption model of gas/particle partitioning of organic compounds in the atmosphere, *Atmos. Environ.*,  
28, 185-188, 1994.
- 335 Paulson, S. E., and Orlando, J. J.: The reactions of ozone with alkenes: An important source of HO<sub>x</sub> in the boundary layer,  
*Geophys. Res. Lett.*, 23, 3727-3730, <https://doi.org/10.1029/96GL03477>, 1996.
- Ran, L., Deng, Z., Xu, X., Yan, P., Lin, W., Wang, Y., Tian, P., Wang, P., Pan, W., and Lu, D.: Vertical profiles of black  
carbon measured by a micro-aethalometer in summer in the North China Plain, *Atmos. Chem. Phys.*, 16, 10441-10454,  
10.5194/acp-16-10441-2016, 2016.
- 340 Riipinen, I., Pierce, J. R., Yli-Juuti, T., Nieminen, T., Häkkinen, S., Ehn, M., Junninen, H., Lehtipalo, K., Petäjä, T., Slowik,  
J., Chang, R., Shantz, N. C., Abbatt, J., Leaitch, W. R., Kerminen, V. M., Worsnop, D. R., Pandis, S. N., Donahue, N. M.,  
and Kulmala, M.: Organic condensation: a vital link connecting aerosol formation to cloud condensation nuclei (CCN)  
concentrations, *Atmos. Chem. Phys.*, 11, 3865-3878, 10.5194/acp-11-3865-2011, 2011.
- Riipinen, I., Yli-Juuti, T., Pierce, J. R., Petäjä, T., Worsnop, D. R., Kulmala, M., and Donahue, N. M.: The contribution of  
345 organics to atmospheric nanoparticle growth, *Nat. Geosci.*, 5, 453-458, 10.1038/ngeo1499, 2012.
- Robinson, A., Donahue, N., Shrivastava, M., Weitkamp, E., Sage, M., Grieshop, A., Lane, T., Pierce, J., and Pandis, S.:  
Rethinking Organic Aerosols: Semivolatile Emissions and Photochemical Aging, *Science*, 315, 1259-1262,  
10.1126/science.1133061, 2007.
- Salo, K., Westerlund, J., Andersson, P. U., Nielsen, C., D'Anna, B., and Hallquist, M.: Thermal Characterization of  
350 Aminium Nitrate Nanoparticles, *J. PHYS. CHEM. A*, 115, 11671-11677, 10.1021/jp204957k, 2011.
- Schurman, M. I., Lee, T., Sun, Y., Schichtel, B. A., Kreidenweis, S. M., and Collett Jr, J. L.: Investigating types and sources  
of organic aerosol in Rocky Mountain National Park using aerosol mass spectrometry, *Atmos. Chem. Phys.*, 15, 737-752,  
10.5194/acp-15-737-2015, 2015.
- Shrivastava, M., Cappa, C. D., Fan, J., Goldstein, A. H., Guenther, A. B., Jimenez, J. L., Kuang, C., Laskin, A., Martin, S. T.,  
355 Ng, N. L., Petaja, T., Pierce, J. R., Rasch, P. J., Roldin, P., Seinfeld, J. H., Shilling, J., Smith, J. N., Thornton, J. A.,  
Volkamer, R., Wang, J., Worsnop, D. R., Zaveri, R. A., Zelenyuk, A., and Zhang, Q.: Recent advances in understanding



- secondary organic aerosol: Implications for global climate forcing, *Rev. Geophys.*, 55, 509-559, 10.1002/2016rg000540, 2017.
- Shrivastava, M. K., Lipsky, E. M., Stanier, C. O., and Robinson, A. L.: Modeling Semivolatile Organic Aerosol Mass  
360 Emissions from Combustion Systems, *Environ. Sci. Technol.*, 40, 2671-2677, 10.1021/es0522231, 2006.
- Sun, Y., Du, W., Fu, P., Wang, Q., Li, J., Ge, X., Zhang, Q., Zhu, C., Ren, L., Xu, W., Zhao, J., Han, T., Worsnop, D. R.,  
and Wang, Z.: Primary and secondary aerosols in Beijing in winter: sources, variations and processes, *Atmos. Chem. Phys.*,  
16, 8309-8329, 10.5194/acp-16-8309-2016, 2016.
- Tang, G., Zhu, X., Hu, B., Xin, J., Wang, L., Munkel, C., Mao, G., and Wang, Y.: Impact of emission controls on air quality  
365 in Beijing during APEC 2014: lidar ceilometer observations, *Atmos. Chem. Phys.*, 15, 12667-12680, 10.5194/acp-15-12667-  
2015, 2015.
- Tsigradis, K., Daskalakis, N., Kanakidou, M., Adams, P., Artaxo, P., Bahadur, R., Balkanski, Y., Bauer, S., Bellouin, N.,  
and Benedetti, A.: The AeroCom evaluation and intercomparison of organic aerosol in global models, *Atmos. Chem. Phys.*,  
14, 10845-10895, 2014.
- 370 Ulbrich, I. M., Canagaratna, M. R., Zhang, Q., Worsnop, D. R., and Jimenez, J. L.: Interpretation of organic components  
from Positive Matrix Factorization of aerosol mass spectrometric data, *Atmos. Chem. Phys.*, 9, 2891-2918, 10.5194/acp-9-  
2891-2009, 2009.
- Van Krevelen, D. W.: Graphical-statistical method for the study of structure and reaction processes of coal, *Fuel*, 24, 269-  
284, 1950.
- 375 Wang, X., Heald, C., Ridley, D., Schwarz, J., Spackman, J., Perring, A., Coe, H., Liu, D., and Clarke, A.: Exploiting  
simultaneous observational constraints on mass and absorption to estimate the global direct radiative forcing of black carbon  
and brown carbon, *Atmos. Chem. Phys.*, 14, 10989-11010, 2014.
- Wu, F., Xie, P., Li, A., Mou, F., Chen, H., Zhu, Y., Zhu, T., Liu, J., and Liu, W.: Investigations of temporal and spatial  
distribution of precursors SO<sub>2</sub> and NO<sub>2</sub> vertical columns in the North China Plain using mobile DOAS, *Atmos. Chem. Phys.*,  
380 18, 1535-1554, 10.5194/acp-18-1535-2018, 2018.
- Xu, W. Q., Sun, Y. L., Chen, C., Du, W., Han, T. T., Wang, Q. Q., Fu, P. Q., Wang, Z. F., Zhao, X. J., Zhou, L. B., Ji, D. S.,  
Wang, P. C., and Worsnop, D. R.: Aerosol composition, oxidation properties, and sources in Beijing: results from the 2014  
Asia-Pacific Economic Cooperation summit study, *Atmos. Chem. Phys.*, 15, 13681-13698, 10.5194/acp-15-13681-2015,  
2015.
- 385 Xu, W. Y., Zhao, C. S., Ran, L., Lin, W. L., Yan, P., and Xu, X. B.: SO<sub>2</sub> noontime-peak phenomenon in the North China  
Plain, *Atmos. Chem. Phys.*, 14, 7757-7768, 10.5194/acp-14-7757-2014, 2014.
- Zhang, J. K., Sun, Y., Liu, Z. R., Ji, D. S., Hu, B., Liu, Q., and Wang, Y. S.: Characterization of submicron aerosols during a  
month of serious pollution in Beijing, 2013, *Atmos. Chem. Phys.*, 14, 2887-2903, 10.5194/acp-14-2887-2014, 2014.
- Zhang, Q., Jimenez, J. L., Canagaratna, M. R., Allan, J. D., Coe, H., Ulbrich, I., Alfarra, M. R., Takami, A., Middlebrook, A.  
390 M., Sun, Y. L., Dzepina, K., Dunlea, E., Docherty, K., DeCarlo, P. F., Salcedo, D., Onasch, T., Jayne, J. T., Miyoshi, T.,



- Shimono, A., Hatakeyama, S., Takegawa, N., Kondo, Y., Schneider, J., Drewnick, F., Borrmann, S., Weimer, S., Demerjian, K., Williams, P., Bower, K., Bahreini, R., Cottrell, L., Griffin, R. J., Rautiainen, J., Sun, J. Y., Zhang, Y. M., and Worsnop, D. R.: Ubiquity and dominance of oxygenated species in organic aerosols in anthropogenically-influenced Northern Hemisphere midlatitudes, *Geophys. Res. Lett.*, 34, L13801, 10.1029/2007gl029979, 2007.
- 395 Zhang, Q., Jimenez, J., Canagaratna, M., Ulbrich, I., Ng, N., Worsnop, D., and Sun, Y.: Understanding atmospheric organic aerosols via factor analysis of aerosol mass spectrometry: a review, *Anal. Bioanal. Chem.*, 401, 3045-3067, 10.1007/s00216-011-5355-y, 2011.
- Zhang, R., Suh, I., Zhao, J., Zhang, D., Fortner, E. C., Tie, X., Molina, L. T., and Molina, M. J.: Atmospheric New Particle Formation Enhanced by Organic Acids, *Science*, 304, 1487-1490, 10.1126/science.1095139 %J Science, 2004.
- 400 Zhang, X. Y., Wang, J. Z., Wang, Y. Q., Liu, H. L., Sun, J. Y., and Zhang, Y. M.: Changes in chemical components of aerosol particles in different haze regions in China from 2006 to 2013 and contribution of meteorological factors, *Atmos. Chem. Phys.*, 15, 12935-12952, 10.5194/acp-15-12935-2015, 2015.
- Zhao, D., Huang, M., Tian, P., He, H., Lowe, D., Zhou, W., Sheng, J., Wang, F., Bi, K., Kong, S., Yang, Y., Liu, Q., Liu, D., and Ding, D.: Vertical characteristics of black carbon physical properties over Beijing region in warm and cold seasons, *Atmos. Environ.*, 213, 296-310, <https://doi.org/10.1016/j.atmosenv.2019.06.007>, 2019.
- 405

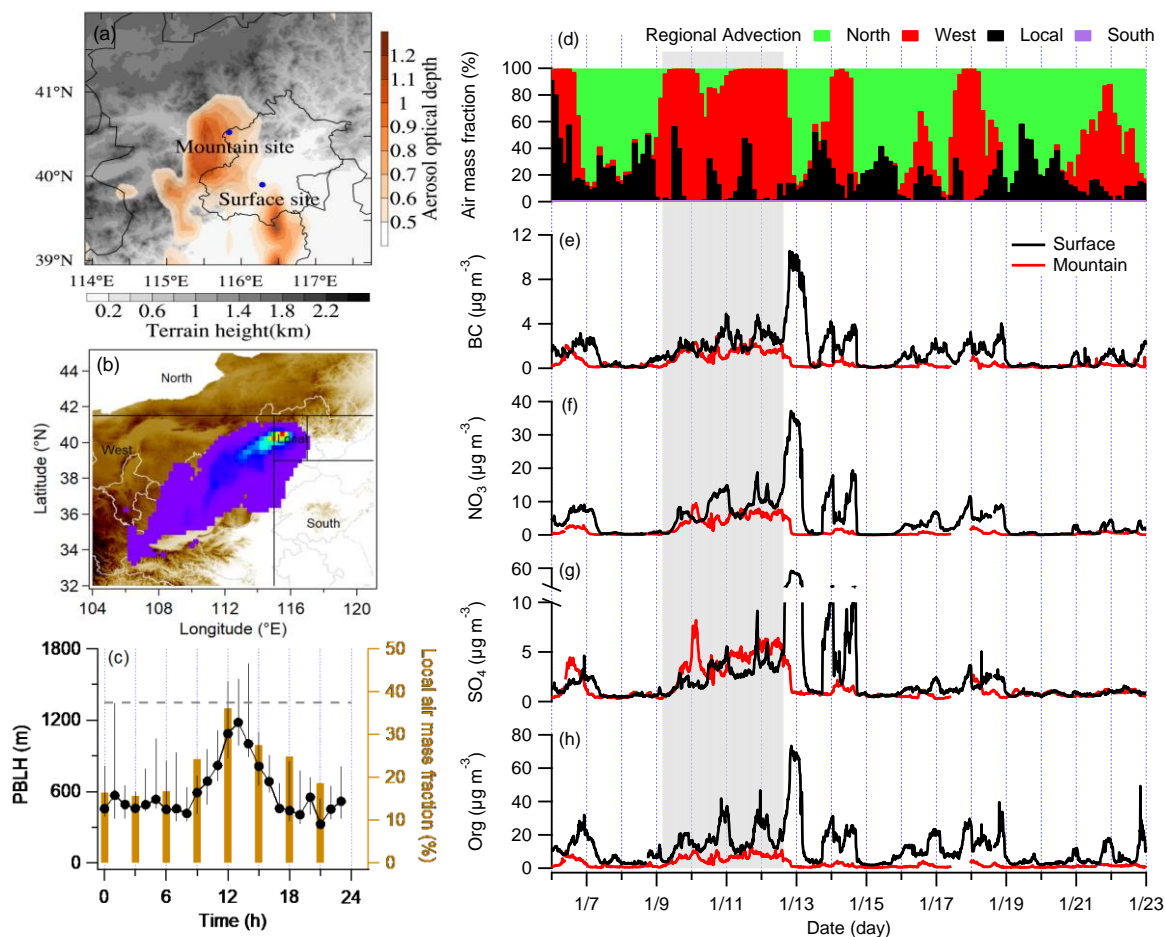


**Fig. 1.** Experimental overview. (a) spatial distribution of mean aerosol optical depth for the experimental month, with  
 410 locations of surface and mountain sites, colored by terrain height; (b) a typical example of westerly dominated air mass from  
 the NAME dispersion model outputs; (c) diurnal cycles of planetary boundary layer height (PBLH) and local air mass  
 fraction contributed to the mountain site during the experimental period, with whiskers showing the 25<sup>th</sup> and 75<sup>th</sup> percentiles;  
 (d) time series of air mass fractions at the mountain; (e-h) time series of black carbon (BC), nitrate (NO<sub>3</sub>), sulfate (SO<sub>4</sub>), and  
 organics (Org), with the black and red lines showing the surface and mountain site respectively.

415

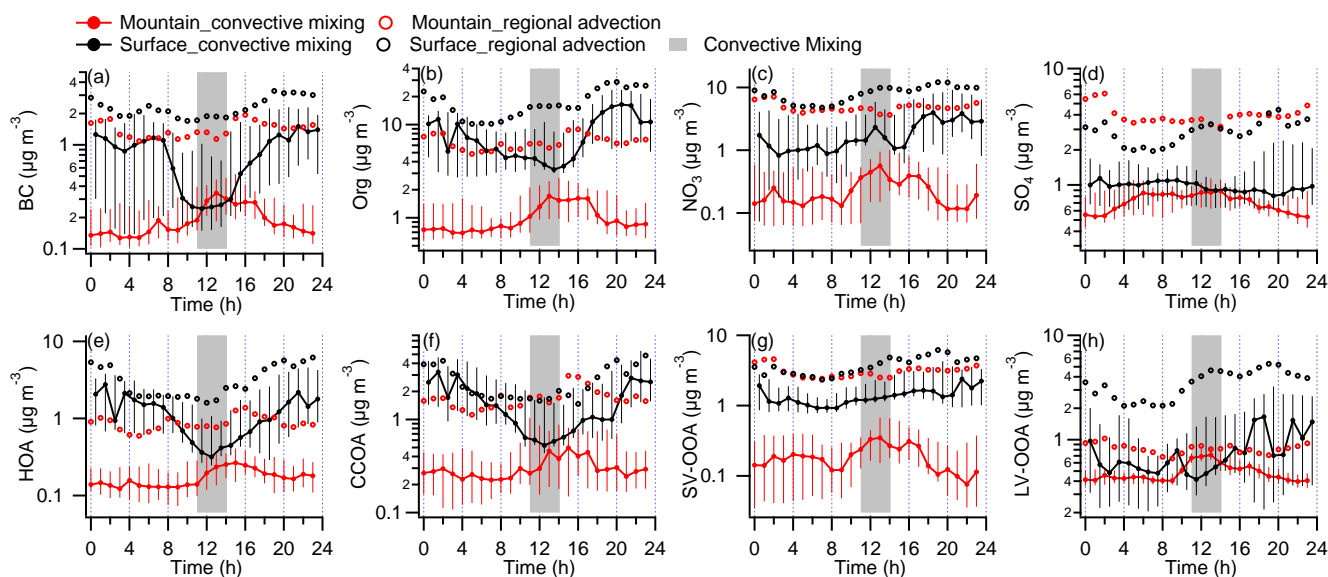


**Fig. 2.** Diurnal variations of key aerosol compositions at both sites during convective mixing (CM) and regional advection (RA) periods, (a) black carbon (BC); (b) organics (Org); (c) nitrate ( $\text{NO}_3$ ); (d) sulfate ( $\text{SO}_4$ ); (e) the sum of hydrocarbon OA (HOA) and cooking related OA (COA); (f) coal combustion-related OA (CCOA); (g) semi-volatile oxygenated OA (SV-OOA); (h) low-volatile oxygenated OA (LV-OOA). The black and red colors represent the surface and mountain site respectively. Solid circles and error bars show the median, 75<sup>th</sup>, and 25<sup>th</sup> percentiles in CM period. Circle markers show the mean value in RA period. Grey bar represents the time in the day (11:00-14:00) with most developed PBL.



425

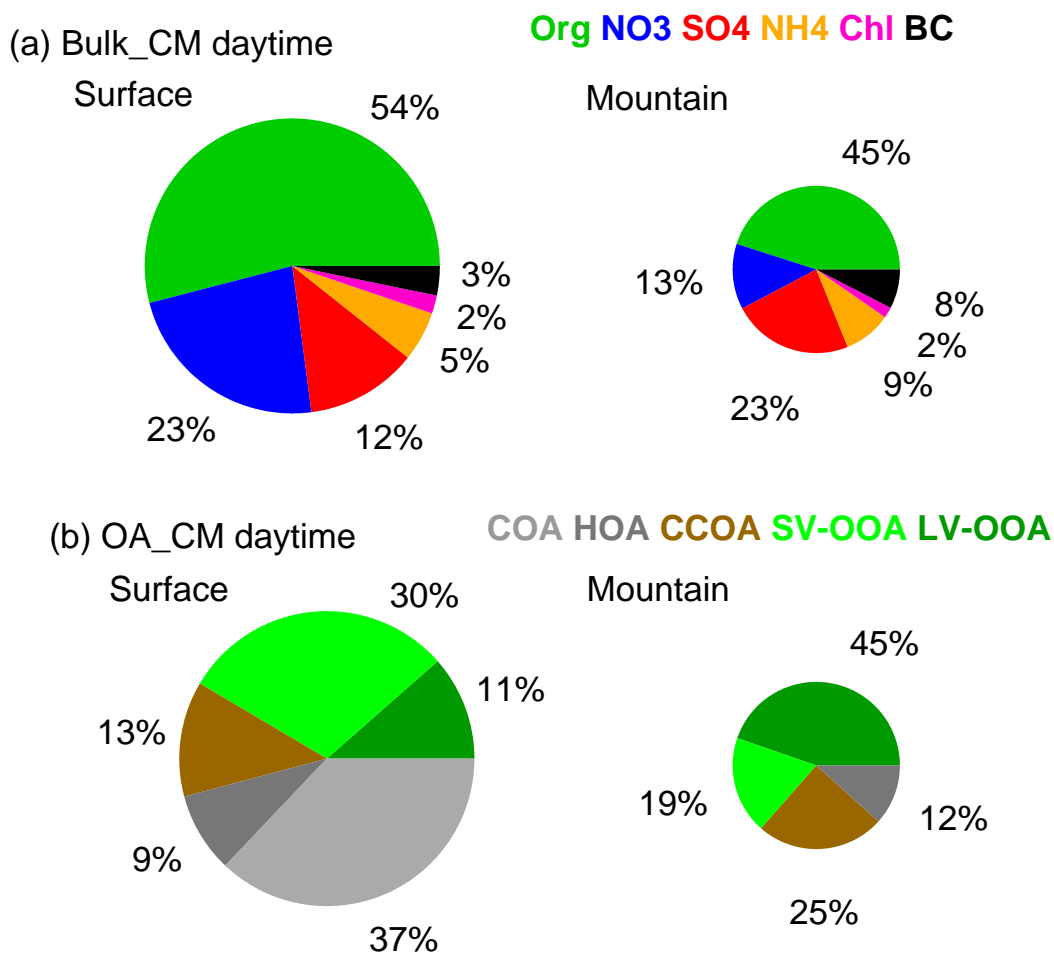


**Fig. 3.** Averaged chemical composition at both sites during convective mixing (CM) period daytime (11:00-14:00), (a) bulk aerosols; (b) organic aerosols.

430



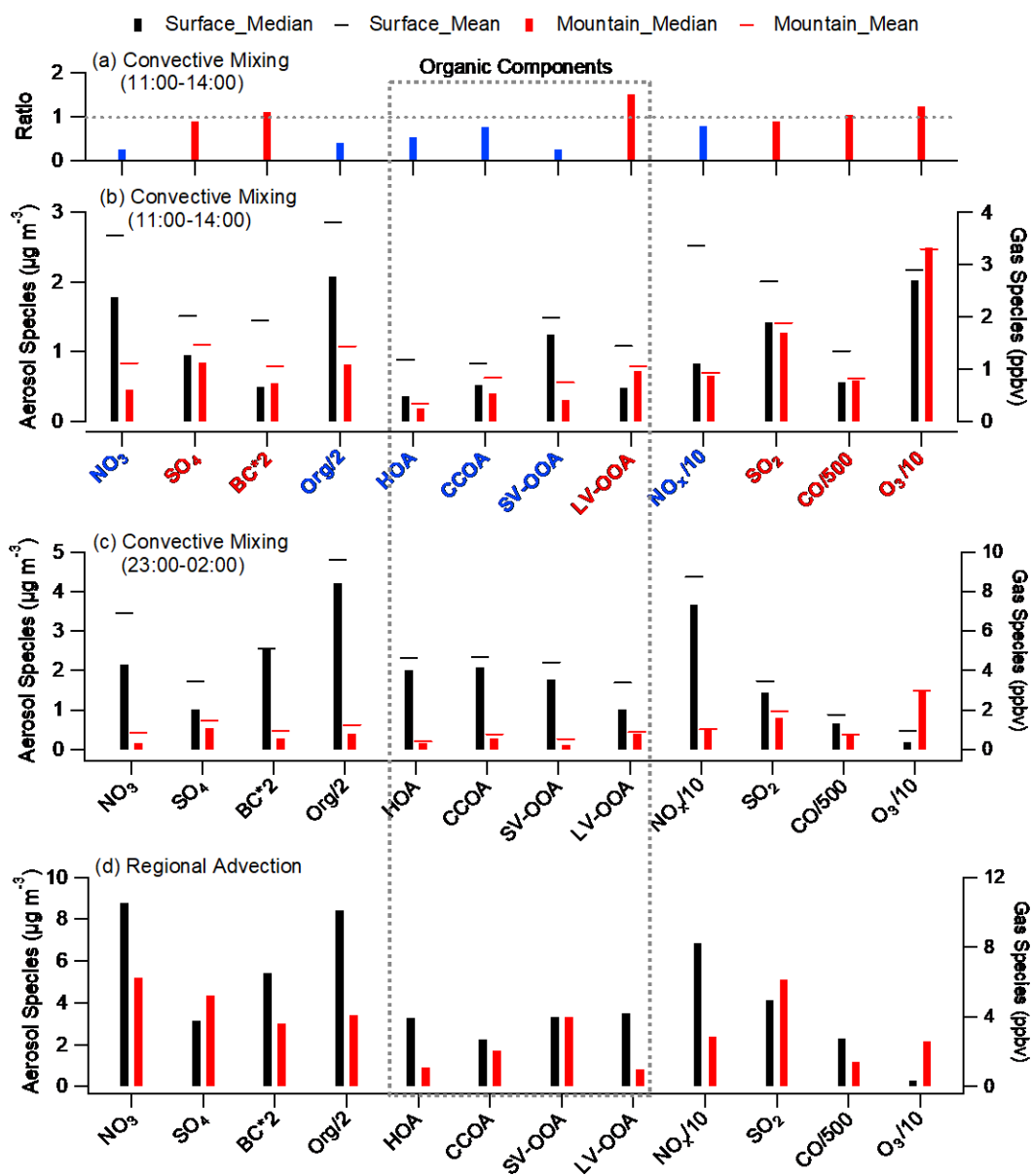


**Fig. 4.** Statistical analysis of chemical components at both sites. (a) the mountain over surface ratio of key species during convective mixing (CM) period daytime (11:00-14:00); (b) median concentrations of key species during CM daytime, with black and red bars denoting the surface and mountain respectively and the cap showing the mean; (c-d) The same with panel b) but for the periods of CM night and RA period. Species with mountain/surface ratio above and below 0.8 are marked in red and blue, respectively.

440

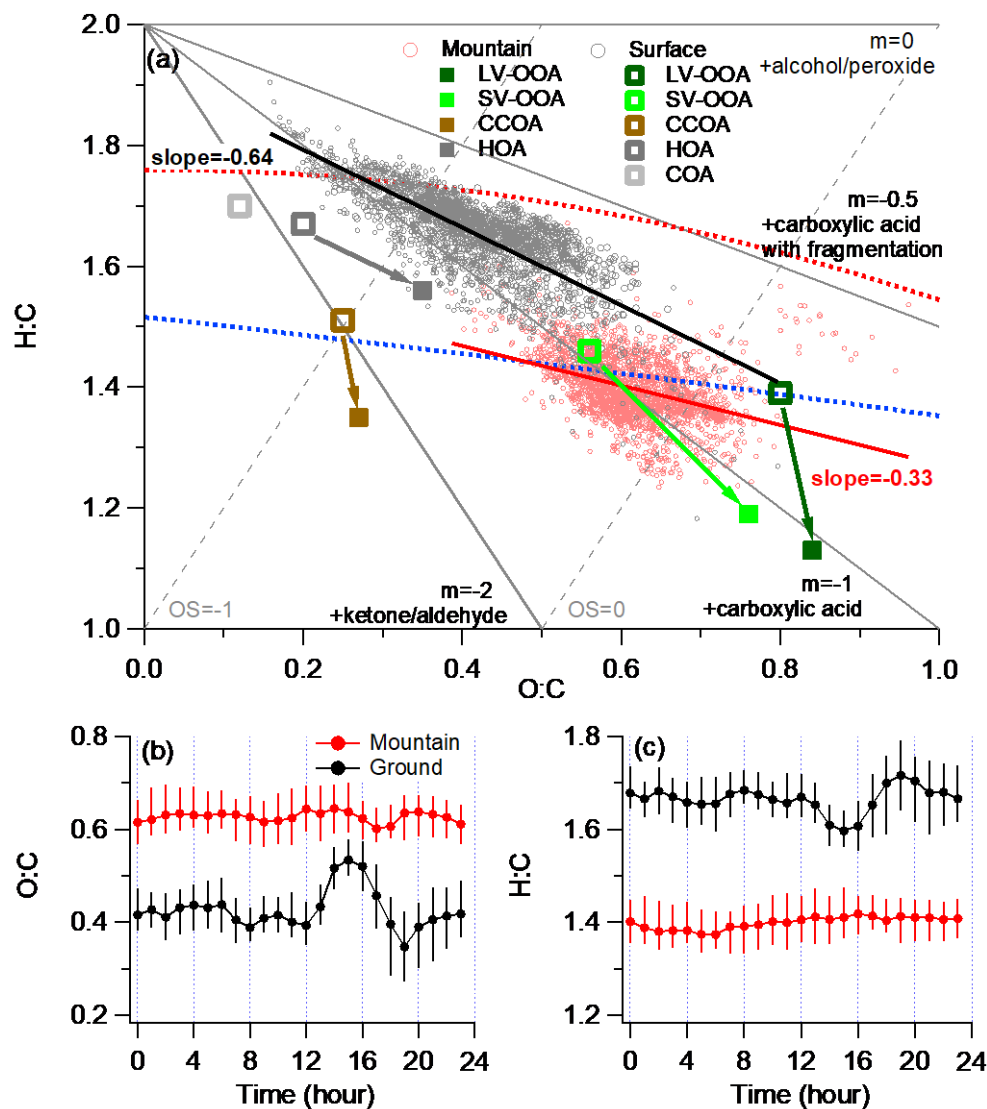


**Fig. 5.** Characterization of elemental ratios at both surface and mountain sites, (a) The standard Van Krevelen-triangle diagram of H:C versus O:C; (b) diurnal variations of O:C; (c) diurnal variations of H:C. The grey and red circles denote the data points from the surface and mountain sites respectively.

445

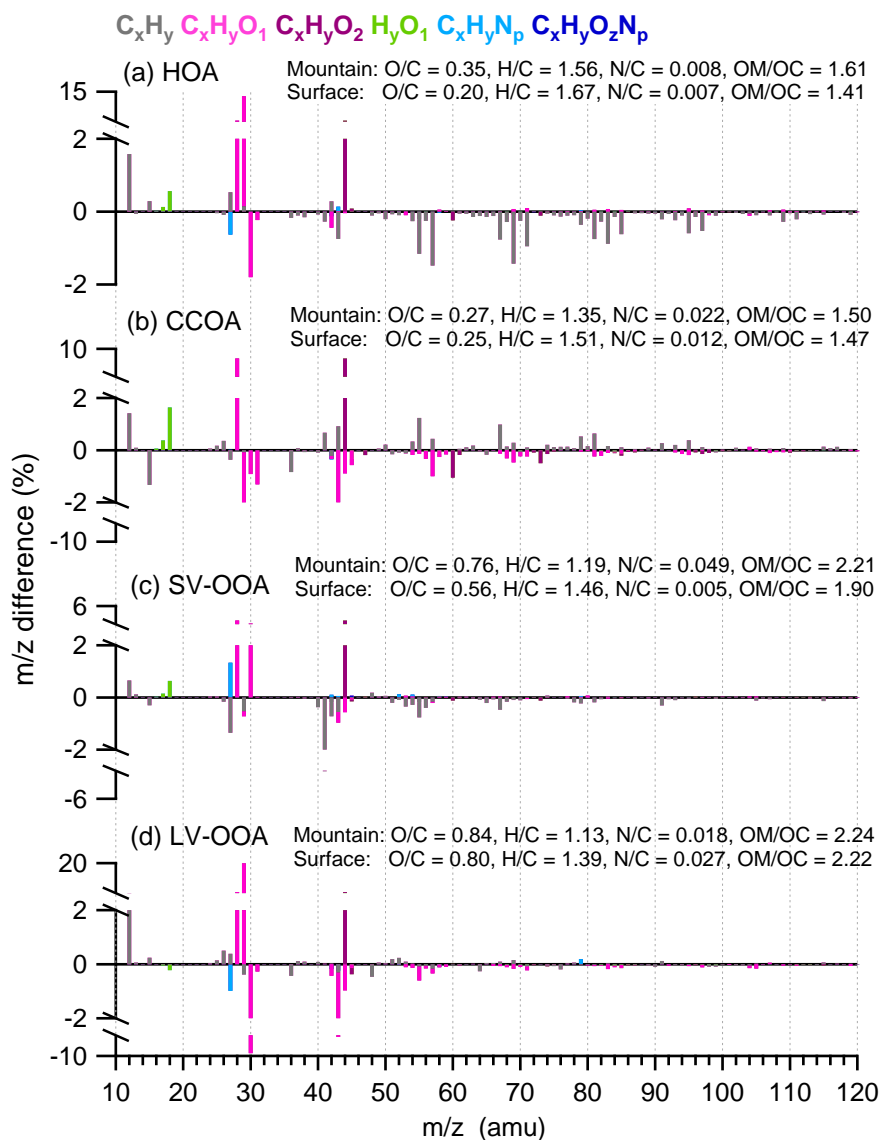


**Fig. 6.** Difference of mass spectra between mountain and surface sites (mountain minus surface) for (a) HOA, (b) CCOA, (c) SV-OOA, and (d) LV-OOA.